Appl Phys B (2009) 94: 175–179
DOI 10.1007/s00340-008-3255-4

Applied Physics B
Lasers and Optics

Filamentation of ultrashort light pulses in a liquid scattering medium

V. Jukna · G. Tamošauskas · G. Valiulis · M. Aputis · M. Puida · F. Ivanauskas · A. Dubietis

Received: 1 July 2008 / Revised version: 3 October 2008 / Published online: 22 October 2008

Abstract We have studied filamentation of 1-ps laser pulses in a scattering medium (aqueous suspension of 2-μm polystyrene microspheres) and compared filamentation dynamics to that in pure water. Our results indicate that light scattering does not alter filamentation dynamics in general, but rather results in farther position of the nonlinear focus, shorter filament length, and the development of speckle structure in the peripheral part of the beam. The experimental observations are qualitatively reproduced by the numerical model which accounts for diffraction, self-focusing, multiphoton absorption, and light scattering introduced through a stochastic diffusion and diffraction term.

PACS 42.65.Jx · 42.25.Bs

1 Introduction

The filamentation of the ultrashort light pulses is an ultimate manifestation of the nonlinear medium response to the intense light field, resulting in contraction and reshaping of the laser beam accompanied by spectral broadening, plasma generation, temporal reshaping, and sub-diffractive propagation [1, 2]. Recent experiments involving near-field detection prove spontaneous transformation of the input Gaussian beam into the nonlinear conical wave driven by complex interplay between self-focusing, nonlinear losses (multiphoton absorption) and diffraction [3]. The conical wave is composed of an intense narrow core (termed a filament), which carries just a small fraction of the total energy, and an extended, low-intensity but high energy reservoir, which travels locked as a single quasistationary profile. Only the intense core interacts nonlinearly with the medium and so experiences nonlinear energy losses, while the extended energy reservoir propagates linearly and continuously refills the core during its propagation. The refilling feature is universal and is observed in transparent solid-state, liquid or gaseous media. To this regard, light filaments were shown to survive the collisions with the filament-size obstacles, such as atmospheric obscurants, aerosols, water droplets [4–6], or artificial opaque screens [7]. By contrast, filament propagation terminates if the extended energy reservoir is blocked [3, 8]. Such a dynamic coexistence of localized and extended counterparts in the conical wave offers many challenging tasks in applied research ranging from atmospheric applications to extended-depth microprocessing of transparent solids.

To date, much effort has been directed to the filamentation in scattering media with implications to long-range propagation, remote sensing and lightning control in adverse atmospheric conditions, in the presence of rain, fog, aerosol scattering, and high turbulence [9–13]; see also [14] for a comprehensive review on the topic. Numerically, light scattering in the atmospheric propagation may be simply simulated by introducing some energy dissipation through linear losses [15] or using a stratified model consisting of a sequence of aerosol screens [16]. On a smaller scale, many questions still remain open concerning the propagation of narrow light beams in biological systems that are transpar-

V. Jukna (✉) · G. Tamošauskas · G. Valiulis · M. Aputis · A. Dubietis
Department of Quantum Electronics, Vilnius University, Saulėtekio Avenue 9, bldg. 3, 10222 Vilnius, Lithuania
e-mail: Vytautas.Jukna@ff.vu.lt

M. Puida · F. Ivanauskas
Faculty of Mathematics and Informatics, Vilnius University, Naugarduko 24, 03225 Vilnius, Lithuania

ent but exhibit strong scattering [17, 18]. To this regard, nonlinear propagation of the ultrashort light pulses in biological systems opens many new challenges, such as localized in-depth nonlinear excitation of biological agents, two-photon microscopy within a tissue, and precise laser cutting [19–21], to mention a few.

In this paper, we report the numerical and experimental results on the picosecond laser pulse filamentation in a liquid scattering medium (aqueous suspension of 2 μm polystyrene microspheres of different concentration). Experimental and numerical results imply that strong scattering leads to distortions of the filament energy reservoir developing an apparent speckle structure, but does not greatly alter filament formation and propagation dynamics.

2 Experiment

The experiment was carried out with chirped-pulse-amplification based Nd:glass laser system (Twinkle, Light Conversion Ltd.) delivering $\lambda = 1054$ nm, 1 ps pulses at 10 Hz repetition rate. The output laser beam was frequency doubled, attenuated and spatially filtered to yield a clean Gaussian profile at $\lambda = 527$ nm with 1.2 mm FWHM diameter. The second-harmonic beam was loosely focused by a $f = +500$ mm lens down to 80 μm FWHM diameter onto the front-face of the syringe-shaped cuvette with fused silica windows. The cuvette was filled either with aqueous suspension of 2 μm diameter calibrated polystyrene microspheres, provided by Vasmo Inc. (Indianapolis, IN) or with pure water for a comparative study. The input pulse energy was set $E_{\text{in}} = 6$ μJ, so as to excite a single filament inside a cuvette filled with pure water at a distance $z = 12$ mm from its front-face. The construction of the cuvette allowed easy varying of its length and monitoring the output beam near-field fluence profile, and therefore capturing in detail the propagation dynamics. In doing so, the output face of the cuvette was imaged onto a 10-bit dynamic range CCD camera (COHU-6612 linked to Spiricon LBA-400PC frame grabber) by means of an achromatic $f = +50$ mm lens, with $7\times$ magnification.

Figure 1 compares beam propagation and filament formation dynamics in the absence (in pure water, Fig. 1(a, c)) and in the presence (in aqueous suspension of 2 μm polystyrene microspheres with 6000 mm^{-3} particle density, Fig. 1(b, d)) of light scattering. The general side-views of a full-length propagation in a 40-mm-long cuvette were taken by a digital photo camera using the same input energy of $E_{\text{in}} = 6$ μJ. The most of scattered light is confined within a cone having vertex angle of 10° indicated by light lines in Fig. 1(b), whereas dark lines denote the scattering angle to half maximum intensity, as calculated using Mie scattering theory [22], and

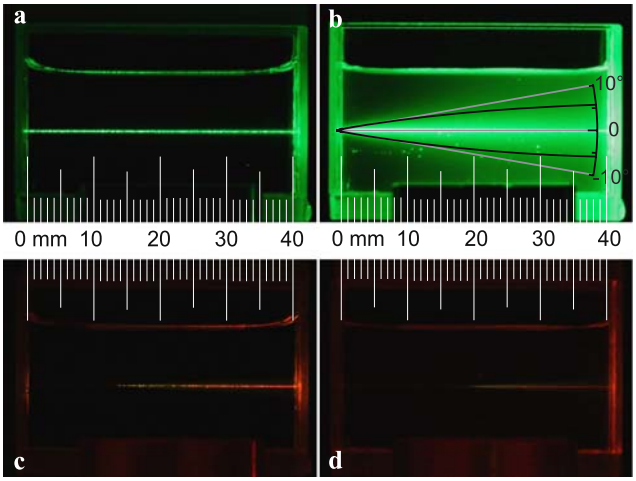

Fig. 1 Side-view of the cuvette in the nonlinear propagation regime at $E_{\text{in}} = 6$ μJ: (**a**) pure water, (**b**) aqueous solution of 2 μm polystyrene microspheres with 6000 mm^{-3} particle density. (**c**) and (**d**) are the respective images recorded using an orange filter

which are in good agreement with the experimental results. Laser beam filamentation is visualized by the appearance of the white-light continuum emission and is detected using an orange filter that transmits only wavelengths longer than 600 nm as shown in Fig. 1(c) and (d). In order to observe an appreciable signal from a side-view in pure water, we have used a very dilute solution of the scatterers in this case and increased the exposure time.

In pure water, beam filamentation starts at $z = 12$ mm from the input face as seen from Fig. 1(c), whereas in the presence of scattering the nonlinear focus and filament start point is shifted towards the output face, and under our experimental settings still occurs within the cuvette length. Typical near-field images of the radiation which was detected by imaging the output face of the cuvette onto a CCD camera and continuously varying the propagation length are shown in Fig. 2. Although the scattering is found to affect the filament start position resulting in somewhat farther point of the nonlinear focus, our observation suggests that even in the presence of strong scattering (energy losses up to 50%) the transverse beam profile, which takes the shape of an intense central core (filament) surrounded by an extended (conical) peripheral radiation is highly resistant to local perturbations imposed by the scatterers. The peripheral part of the radiation develops an apparent speckle structure, which is still able of refilling the nonlinear losses due to multiphoton absorption experienced by the intense central core and linear losses due to scattering experienced by the entire beam. Here we note that the diameter of a single microsphere comprises ∼16% of the estimated filament FWHM width (12 μm).

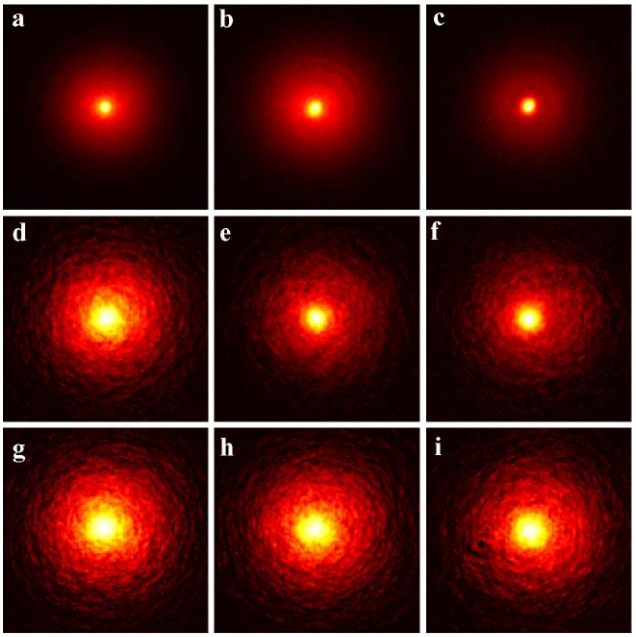

Fig. 2 Experimentally measured single-shot fluence profiles of the beam beyond the nonlinear focus: (**a–c**) in pure water, (**d–f**) in aqueous suspension of the polystyrene microspheres of 6000 mm^{-3}, (**g–i**) in 8000 mm^{-3} aqueous polystyrene microspheres suspension at $z = 12, 16, 20$ mm. Window size is 0.3 mm × 0.3 mm

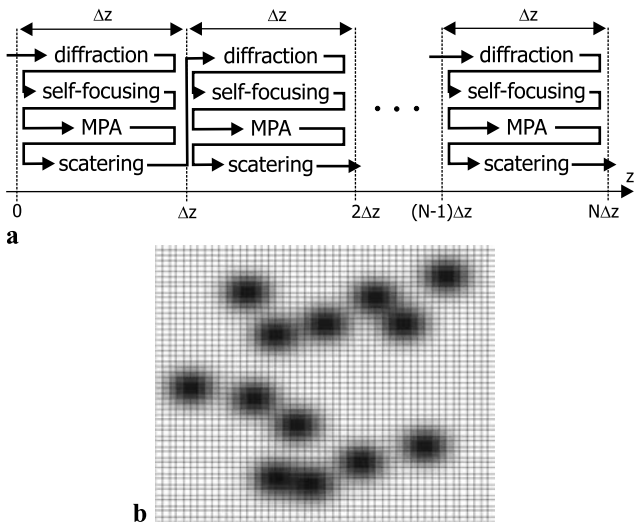

Fig. 3 (**a**) A schematic representation of the numerical procedure, (**b**) an example of the $\gamma(x, y, z)$

3 The model

The propagation in the scattering medium was modeled in the framework of the nonlinear Schroedinger equation for the monochromatic field amplitude A with account for diffraction, self-focusing, multiphoton absorption (MPA) [3], and with addition of a stochastic term which simulates size, properties and distribution of the scattering particles:

$$\frac{\partial A}{\partial z} = \frac{i}{2k}\left(\frac{\partial^2}{\partial x^2} + \frac{\partial^2}{\partial y^2}\right)A + \frac{i\omega n_2}{c}|A|^2 A - \frac{\beta^{(K)}}{2}|A|^{2K-2}A - \gamma A, \quad (1)$$

where z is the propagation distance, ω is the carrier frequency, $k = n\omega/c$ is the wave number, n and n_2 are the linear and nonlinear refractive indexes, respectively, K is the order of multiphoton absorption with $\beta^{(K)}$ being the multiphoton absorption coefficient, and γ is the stochastic complex function (specified in the text below). In our simulation, we used the following values of the relevant parameters $n = 1.33$, $n_2 = 2.7 \times 10^{-16}$ cm^2/W, $K = 3$ (three photon absorption with account of water bandgap $E_g = 6.5$ eV) and $\beta^{(3)} = 2 \times 10^{-23}$ cm^3/W^2 as taken from [23]. Equation (1) was solved by means of the commonly used split-step Fourier method. Specifically, the medium is divided into a number of layers N of arbitrary thickness Δz, and the propagation through each particular layer is simulated a few times. The full numerical procedure is schematically depicted in Fig. 3(a) and is performed as follows: the first pass through the Nth layer calculates the diffraction by solving a simple equation

$$\frac{\partial A}{\partial z} = \frac{i}{2k}\left(\frac{\partial^2}{\partial x^2} + \frac{\partial^2}{\partial y^2}\right)A \quad (2)$$

using the fast Fourier transform algorithm. Thereafter, the same layer is passed again, but now accounting for the self-focusing:

$$\frac{\partial A}{\partial z} = \frac{i\omega n_2}{c}|A|^2 A. \quad (3)$$

The third passage accounts for the multiphoton absorption:

$$\frac{\partial A}{\partial z} = -\frac{\beta^{(K)}}{2}|A|^{2K-2}A, \quad (4)$$

and the last one for scattering:

$$\frac{\partial A}{\partial z} = -\gamma A, \quad (5)$$

where $\gamma(x, y, z)$ is a complex matrix representing properties and location of randomly distributed scattering particles. Specifically, its real part, $\mathrm{Re}[\gamma(x, y)]$, describes the absorption, while its imaginary part, $\mathrm{Im}[\gamma(x, y)]$, describes the phase shift (dephasing) introduced by a scattering particle. More generally, for the nth layer, $\gamma(x, y, z_n)$ represents a matrix of random complex values, characterizing the properties of the scatterers: concentration, size and opacity, as illustrated in Fig. 3(b). The calculation procedure is repeated within the next layer, with the last step involving the generation of a new matrix $\gamma(x, y, z_n)$, which keeps particle properties fixed and changing just their spatial distribution.

The layer thickness Δz in our calculations was chosen to be an average distance between the scattering particles, that is, ∼45–55 μm for the scattering particle concentration of 10000 to 6000 cm^{-3}. The grid size in the (x, y) plane was 0.2 mm × 0.2 mm, with 0.4 μm resolution and 2^{18} pixels.

Since the actual properties of the scattering particles (refractive index, absorption, etc.) were not provided by the producer, the actual extinction experienced by the laser beam was estimated from the energy loss due to scattering in the linear propagation regime of an extended Gaussian beam with wavelength 527 nm, which had power well below the critical power for self-focusing. Experimentally, energy losses due to scattering for 6000, 8000, and 10000 mm^{-3} particle density were estimated to be 40%, 49%, and 57%, respectively, as measured in 10-mm-long cuvette. In this measurement, we used a 10-mm diameter iris aperture centered on the beam propagation axis and Ophir Optronics energy meter with a photodiode head PE-10. An iris aperture was placed at 1 m distance after the cuvette, so as to detect the axial energy confined within an angle of 10 mrad. The measured energy losses corresponded to an extinction coefficient of 0.051, 0.0673, and 0.0844 mm^{-1}, respectively, for particle concentrations indicated above. These values were used for the model calibration.

4 Results and summary

Although our model is for monochromatic (continuous) waves and it does not account for more specific features of the nonlinear medium owing to effective nonlinear refractive index [24], effects of scattering on the pulse duration [25] and morphologic dependent resonances in the polystyrene microspheres giving rise to excitation of whispering gallery modes [26], we obtained a good qualitative agreement between the numerical and experimental data. Figure 4 compares the simulated and experimentally measured fluence profiles of the beam after 20 mm of propagation in aqueous suspension of polystyrene microspheres with 8000 mm^{-3} particle density outlining a development of apparent speckle structure in both cases. The only difference is observed in the far periphery because a portion of scattered light at large angles is not collected in the imaging lens in the experiment. Figure 5 (a) compares measured and numerically simulated filamentation dynamics (diameter of the central core, i.e., filament *versus* propagation distance).

In the simulation, the 2 μm-particle introduces strong diffraction, and the Fourier transform algorithm fails when the diffracted light reaches the boundaries of the calculation window. We solved this problem in two different ways: (i) by introducing a spatial filter after passing each layer. The spatial filter cuts high frequency spatial components, having no effect on the central part of the beam; (ii) by replacing

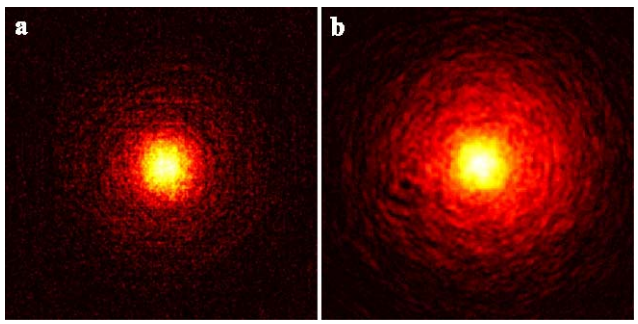

Fig. 4 A comparison of (**a**) simulated and (**b**) experimentally measured beam profiles after 20 mm propagation in aqueous suspension of polystyrene microspheres with 8000 mm^{-3} particle density. Window size is 0.3 mm × 0.3 mm

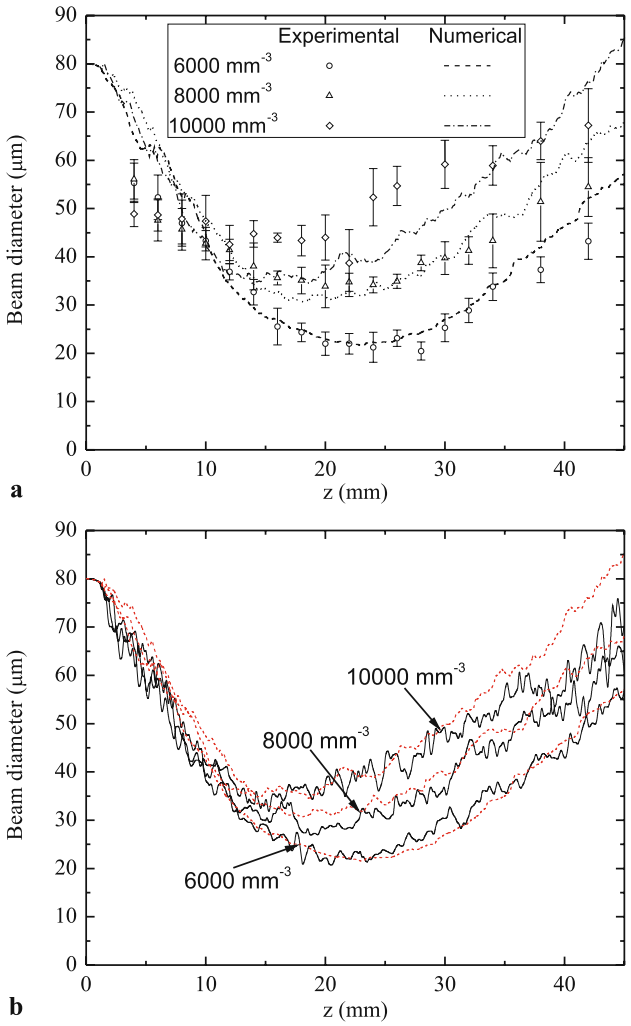

Fig. 5 (**a**) A comparison of the experimental data with numerical simulations of the filament diameter during propagation in aqueous suspension of 2-μm polystyrene microspheres of different concentration. (**b**) A comparison of numerical results obtained with a different computation algorithm, *solid curves*—introducing spatial filter, *dotted curves*—with larger effective particles. See text for details

the scattering particles with the effective ones, which are larger in size and posses some effective absorption. In this case, larger particles introduce smaller diffraction, so that the diminished scattering losses are "compensated" by the absorption. In the latter case, we have used the effective particles of 16 μm in diameter and having 0.15 mm^{-1} absorption coefficient. The comparison between the two simulation approaches is illustrated in Fig. 5(b). It can be seen that both algorithms provide a very similar result concerning the beam diameter, where a slight difference might be recognized only for larger particle concentration and for longer propagation distance. However, in the case of effective particles, the speckle structure is less developed and thus leads to a smoother evolution of the beam diameter.

In conclusion, we have investigated filamentation dynamics of the ultrashort light pulses in a liquid scattering medium. It is shown that light scattering introduced by the polystyrene microspheres shifts the nonlinear focus (emergence of the filament) toward further propagation distance, and results in somewhat larger filament diameter along with appearance of speckle structure in the peripheral part of the beam. The developed monochromatic model, which accounts for diffraction, self-focusing, multiphoton absorption and light scattering, qualitatively reproduces the relevant propagation features observed experimentally with picosecond light pulses. The model is flexible in choosing the parameters of scattering particles (density, size and transparency) and could be easily adopted to any other scattering medium.

References

1. A. Couairon, A. Mysyrowicz, Phys. Rep. **441**, 47 (2007)
2. L. Bergé, S. Skupin, R. Nuter, J. Kasparian, J.-P. Wolf, Rep. Prog. Phys. **70**, 1633 (2007)
3. A. Dubietis, E. Gaižauskas, G. Tamošauskas, P. Di Trapani, Phys. Rev. Lett. **92**, 253903 (2004)
4. F. Courvoisier, V. Boutou, J. Kasparian, E. Salmon, G. Méjean, J. Yu, J.P. Wolf, Appl. Phys. Lett. **83**, 213 (2003)
5. M. Kolesik, J.V. Moloney, Opt. Lett. **29**, 590 (2004)
6. S. Skupin, L. Bergé, U. Peschel, F. Lederer, Phys. Rev. Lett. **93**, 023901 (2004)
7. A. Dubietis, E. Kučinskas, G. Tamošauskas, E. Gaižauskas, M.A. Porras, P. Di Trapani, Opt. Lett. **29**, 2893 (2004)
8. W. Liu, J.-F. Gravel, F. Théberge, A. Becker, S.L. Chin, Appl. Phys. B **80**, 857 (2005)
9. G. Méchain, G. Méjean, R. Ackermann, P. Rohwetter, Y.-B. André, J. Kasparian, B. Prade, K. Stelmaszczyk, J. Yu, E. Salmon, W. Winn, L.A. Schlie, A. Mysyrowicz, R. Sauerbrey, L. Wöste, J.-P. Wolf, Appl. Phys. B **80**, 785 (2005)
10. R. Ackermann, K. Stelmaszczyk, P. Rohwetter, G. Méjean, E. Salmon, J. Yu, J. Kasparian, G. Méchain, V. Bergmann, S. Schaper, B. Weise, T. Kumm, K. Rethmeier, W. Kalkner, L. Wöste, J.-P. Wolf, Appl. Phys. Lett. **85**, 5781 (2004)
11. R. Ackermann, G. Mejean, J. Kasparian, J. Yu, E. Salmon, J.-P. Wolf, Opt. Lett. **31**, 86 (2006)
12. A.A. Zemlyanov, Y.E. Geints, Opt. Commun. **259**, 799 (2006)
13. A.A. Zemlyanov, Y.E. Geints, Commun. **270**, 47 (2007)
14. J. Kasparian, J.-P. Wolf, Opt. Express **16**, 466 (2008)
15. G. Méjean, J. Kasparian, J. Yu, E. Salmon, S. Frey, J.-P. Wolf, S. Skupin, A. Vinçotte, R. Nuter, S. Champeaux, L. Bergé, Phys. Rev. E **72**, 026611 (2005)
16. V.P. Kandidov, V.O. Militsin, Appl. Phys. B **83**, 171 (2006)
17. W.-F. Cheong, S.A. Prahl, A.J. Welsh, IEEE J. Quantum Electron. **26**, 2166 (1990)
18. A. Yodh, B. Chance, Phys. Today **48**(3), 34 (1995)
19. J. Squier, Opt. Photon. News **13**(4), 41 (2002)
20. P.S. Tsai, B. Friedman, J. Squier, D. Kleinfeld, Opt. Photon. News **15**(7), 24 (2004)
21. R. Cicchi, F.S. Pavone, D. Massi, D.D. Sampson, Opt. Express **13**, 2337 (2005)
22. S. Prahl, Mie scattering calculator, http://omlc.ogi.edu/calc/mie_calc.html
23. A. Dubietis, A. Couairon, E. Kučinskas, G. Tamošauskas, E. Gaižauskas, D. Faccio, P. Di Trapani, Appl. Phys. B **84**, 439 (2006)
24. A. Ashkin, J.M. Dziedzic, P.W. Smith, Opt. Lett. **7**, 276 (1982)
25. C. Calba, C. Rozé, T. Girasole, L. Méès, Opt. Commun. **265**, 373 (2006)
26. L.I. Deych, C. Scmidt, A. Chipouline, T. Pertsch, A. Tunnermann, Appl. Phys. B **93**, 21 (2008)